Chemical Science

rsc.li/chemical-science

EDGE ARTICLE
Lei Zhang, Canzhong Lu, Shengqian Ma *et al.*
A window-space-directed assembly strategy for
the construction of supertetrahedron-based zeolitic
mesoporous metal–organic frameworks with
ultramicroporous apertures for selective gas adsorption

ROYAL SOCIETY
OF **CHEMISTRY**

A window-space-directed assembly strategy for the construction of supertetrahedron-based zeolitic mesoporous metal–organic frameworks with ultramicroporous apertures for selective gas adsorption†

Lei Zhang,[*abcd] Fangfang Li,[ad] Jianjun You,[ad] Nengbin Hua,[ad] Qianting Wang,[ad] Junhui Si,[ad] Wenzhe Chen,[ad] Wenjing Wang, [b] Xiaoyuan Wu, [b] Wenbin Yang, [b] Daqiang Yuan, [b] Canzhong Lu, [*be] Yanrong Liu, [f] Abdullah M. Al-Enizi, [g] Ayman Nafady[g] and Shengqian Ma [*c]

Despite their scarcity due to synthetic challenges, supertetrahedron-based metal–organic frameworks (MOFs) possess intriguing architectures, diverse functionalities, and superb properties that make them in-demand materials. Employing a new window-space-directed assembly strategy, a family of mesoporous zeolitic MOFs have been constructed herein from corner-shared supertetrahedra based on homometallic or heterometallic trimers $[M_3(OH/O)(COO)_6]$ ($M_3 = Co_3$, Ni_3 or Co_2Ti). These MOFs consisted of close-packed truncated octahedral cages possessing a sodalite topology and large β-cavity mesoporous cages (∼22 Å diameter) connected by ultramicroporous apertures (∼5.6 Å diameter). Notably, the supertetrahedron-based sodalite topology MOF combined with the Co_2Ti trimer exhibited high thermal and chemical stability as well as the ability to efficiently separate acetylene (C_2H_2) from carbon dioxide (CO_2).

Introduction

Metal–organic frameworks (MOFs),[1] which are typically obtained *via* the self-assembly of metal ions/clusters and organic ligands through coordination bonds, have been a topic of research due to their great potential for various applications, including gas storage and separation,[2,3] heterogeneous

catalysis,[4,5] enzyme immobilization[6,7] and others. The properties of MOFs are highly dependent on the inherent network topologies, which, in turn, are strongly influenced by the coordination geometry of the metal nodes and the shape of the component organic ligands.[8,9] These fascinating MOF network topologies are designed and constructed using numerous rational approaches,[10–12] of which the strategy employing supermolecular building blocks (SBBs) is a most popular one; here, metal–organic polyhedra are used as building blocks to assemble MOFs with large cavities and high-connectivity network topologies.[13,14] Supertetrahedron (ST),[15–17] which is an enlarged SiO_4 and AlO_4 tetrahedral building unit of traditional inorganic zeolites, is a widely utilized SBB in MOF synthesis. Two of the most extensively studied mesoporous MOFs (MIL-100 and MIL-101) possess the same **mtn** zeolite topology, which results from corner-sharing STs whose vertices are occupied by chromium trimers.[15,16] The presence of metal trimers in MOFs are known to accommodate single or multiple metal ions that exhibit excellent catalytic performance and exceptional gas adsorption and separation abilities.[18–21] Of the numerous zeolitic network topologies reported, only two types can be categorized as zeolitic MOFs due to augmentation by STs based on metal trimers, namely, the **mtn**[15,16,22] and β-cristobalite networks.[17,23,24] This could be presumably due to the lack of large, high-quality crystals for single-crystal X-ray

aCollege of Materials Science and Engineering, Fujian University of Technology, Fuzhou 350118, China. E-mail: leizhang@fjut.edu.cn

bCAS Key Laboratory of Design and Assembly of Functional Nanostructures, Fujian Provincial Key Laboratory of Nanomaterials, Fujian Institute of Research on the Structure of Matter, Chinese Academy of Sciences, Fuzhou 350002, China. E-mail: czlu@fjirsm.ac.cn

cDepartment of Chemistry, University of North Texas, Denton 76201, USA. E-mail: Shengqian.Ma@unt.edu

dCollaborative Innovation Center for Intelligent and Green Mold and Die of Fujian Province, Fuzhou 350118, China

eXiamen Institute of Rare Earth Materials, Chinese Academy of Sciences, Xiamen 361021, China

fEnergy Engineering, Division of Energy Science, Luleå University of Technology, Luleå 97187, Sweden

gDepartment of Chemistry, College of Science, King Saud University, Riyadh 11451, Saudi Arabia

† Electronic supplementary information (ESI) available. CCDC 2026913–2026915. For ESI and crystallographic data in CIF or other electronic format see DOI: 10.1039/d0sc06841a

diffraction (SCXRD) analysis and the complexity of the results obtained *via* powder X-ray diffraction (PXRD). Despite the associated challenges, the deliberate introduction of corner-shared STs based on metal trimers into MOFs with other zeolitic network topologies, especially those containing suitably sized single-crystals for SCXRD, is a crucial step toward understanding these materials.

The most thoroughly studied zeolitic imidazole framework to date is ZIF-8, which possesses a sodalite (**sod**) topology with a Brunauer–Emmett–Teller (BET) surface area of 1630 m^2 g^{-1}.[25,26] ZIF-8 contains large β-cavities of approximately 11.6 Å in diameter that are accessible through narrow hexagonal windows. The square window of the β-cavity has a negligible diameter, whereas the hexagonal window is 3.4 Å in diameter. Significantly, ZIF-8 has a high uptake capacity as a result of its higher surface area and pore volume when compared with traditional inorganic zeolites. Furthermore, the presence of the ultramicroporous aperture in ZIF-8 facilitates its application for hydrocarbon separation *via* a molecular sieving effect.[27,28] On the other hand, MOFs with the ultra-micropore scale (*i.e.*, <7 Å) pore sizes are endowed with strong van der Waals interactions with adsorbed gas molecules.[29,30] Therefore, the combination of ultramicroporous aperture, high surface area and pore volume could lead to the high gas storage and separation ability of MOFs. The adsorption capacity can be enhanced by extending the pore diameters of the β-cavities from the micro-to the mesoscale. However, this process is often compensated by enlarging the windows of the **sod** cage to afford pore apertures that are beyond the ultra-micropore scale, thereby weakening the interactions with gas molecules. We speculate that this issue can be addressed by partially closing the windows of the **sod** cage to retain ultramicroporous aperture thus strengthening the interactions with gas molecules during gas separation procedures. In principle, a **sod** cage with mesoporous β-cavities can be built by closing the large hexagonal window while keeping the small square window open. Such modification to the **sod** cage can maintain exceptionally large β-cavities for improved adsorption meanwhile reduce the pore aperture size to below 7 Å for the efficient separation of mixtures. Therefore, it is anticipated that this approach can circumvent the issues arising from the trade-off between higher adsorption capacity and better selectivity of the respective adsorbents.

The pore-space-partition (PSP) approach conceived by Bu features the division of a large cage or channel space into smaller segments by inserting pore-partitioning agents.[31,32] The PSP approach significantly increases the stability of the framework and improves gas adsorption and separation.[31–35] The C_3 symmetric 2,4,6-tri(4-pyridyl)-1,3,5-triazine (tpt) ligand is often used as a pore-partitioning ligand that can be arranged within the windows of various crystalline molecular cages or cage-based MOFs.[33,36–38]

In this study, an alternative strategy based on the window-space-directed assembly (WSDA) approach is proposed; herein, the windows of the large cage are partially blocked to afford ultramicropore apertures and enhance the host–guest interactions that exist between the host frameworks and the guest molecules. As a proof-of-concept, we designed and

synthesized a series of mixed-linker ST-based **sod**-topology MOFs [M$_3$(OH/O)(H$_2$O)(btc)$_2$(tpt)$_{2/3}$] (ST-**sod**-MOFs) containing 1,3,5-benzenetricarboxylate (btc), 2,4,6-tri(4-pyridyl)-1,3,5-triazine (tpt), homometallic trimer clusters (M$_3$) such as Co$_3$ (ST-**sod**-Co) and Ni$_3$ (ST-**sod**-Ni), and a heterometallic trimer cluster composed of Co$_2$Ti (ST-**sod**-Co/Ti); the MOFs generated featured ultramicroporous square windows and a mesoporous **sod** cage. In these MOFs, STs serve as corner-sharing SBBs to produce a **sod** net topology, and the paired tpt ligands act as window-space-directing agents located on the large hexagonal windows of the **sod** cage. Notably, the mesoporous ST-**sod**-Co/Ti product exhibited high thermal/chemical stability and demonstrated good performance in the separation of acetylene from carbon dioxide.

Results and discussion

The synthesis of the ST-**sod**-MOFs series were conducted by mixing of inorganic salts (CoSO$_4$·7H$_2$O or Ni(NO$_3$)$_2$·6H$_2$O or CoCl$_2$·6H$_2$O and Cp$_2$TiCl$_2$), btc, and tpt with a 9 : 2 : 6 stoichiometric ratio under solvothermal reaction. All three compounds are isostructural frameworks with homo- or heterometallic trimer clusters. The introduction of highly charged Ti^{4+} metals in the metal trimers is anticipated to render high thermal and chemical stability due to thermodynamic parameters.[19,35] The use of tetravalent Ti^{4+} precursor and divalent Co^{2+} precursor afforded heterometallic [Co$_2$Ti(μ$_3$-O)(COO)$_6$] clusters, which were determined by site occupancy refinement and further confirmed by energy dispersive X-ray spectroscopy analysis with the Co/Ti molar ratio (2 : 1) (Fig. S6†). The [Co$_3$(OH)(H$_2$O)(btc)$_2$(tpt)$_{2/3}$] (ST-**sod**-Co) is discussed in detail here (Fig. 1). The SCXRD data analysis revealed that ST-**sod**-Co crystallized in the cubic space group $Im\bar{3}m$. The lattice parameter of $a = b = c = 33.2828(3)$ Å was much longer than that of ZIF-8 (*ca.* 16.9910(1) Å). The secondary building units of ST-**sod**-Co are classic cobalt trimers [Co$_3$(OH)(COO)$_6$] that are connected by four btc ligands to form a ST with a cavity diameter of approximately 4.8 Å; here, the metal trimers and btc ligands were located at the vertices and four faces, respectively (Fig. 1b). The corner-sharing approach caused the STs to assemble into a three-periodic zeolitic **sod** topology framework featuring a large truncated octahedral **sod** cage with a diameter of about 22 Å (Fig. 1c and 2c) that is almost double the size of that observed in ZIF-8 (*ca.* 11.6 Å). Additionally, the larger hexagonal windows of the **sod** cages were occupied by π–π interaction paired tpt ligands, thereby leaving the relatively smaller square windows open (Fig. 1d, 2a and b). The large β-cavities are accessible *via* six square windows with ultramicroporous aperture dimensions of 5.57 × 5.57 Å^2 (Fig. 2a). Thus, the overall structure of ST-**sod**-Co could be viewed as close-packed, large truncated octahedral **sod** cages, each of which possessed eight closed hexagonal windows and six open square windows (Fig. 1d and e).

From a topological viewpoint, the [Co$_3$(OH)(COO)$_6$] clusters and the ligands (btc and tpt) could be reduced to yield 8-, 3-, 3-connected nodes, respectively. As a result, the entire ST-**sod**-Co framework could be defined as a very rare trinodal (3,3,8)-
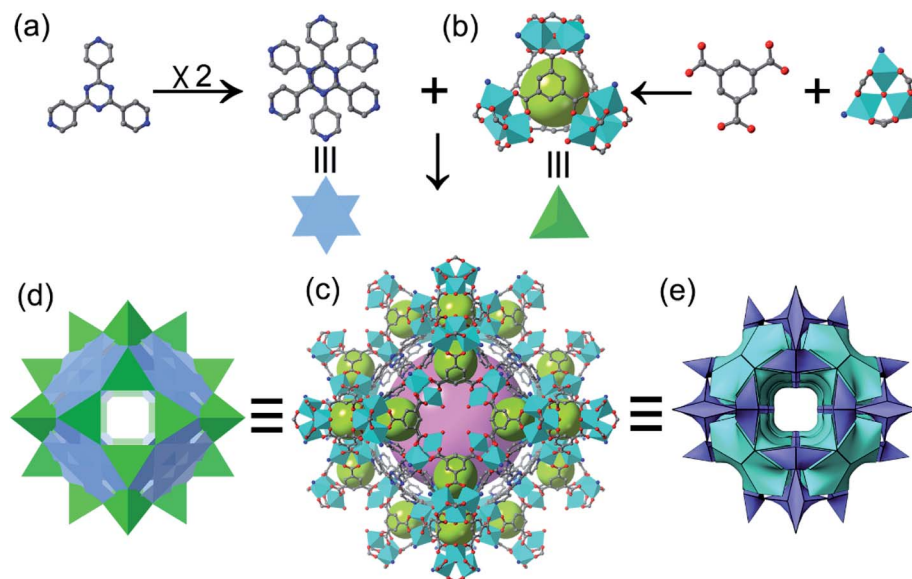
Fig. 1 Schematic of the ST-**sod**-MOF assembly process using ST-**sod**-Co as an example. (a) A pair of staggered tpt ligands were formed *via* $\pi-\pi$ stacking interactions. (b) The ST building block was composed of classic cobalt trimers [Co$_3$(OH)(COO)$_6$] and btc ligands. (c) A β-cavity mesoporous cage in ST-**sod**-Co. (d) ST-**sod**-Co interconnected *via* a **sod** framework with closed hexagonal windows when the STs are considered as nodes. (e) The corresponding tiling model in ST-**sod**-Co. Here, the color code is Co = cyan, C = gray, O = red, and N = blue. Guest molecules and hydrogen atoms have been omitted for clarity. The structure of the cages is illustrated using light pink and green balls.
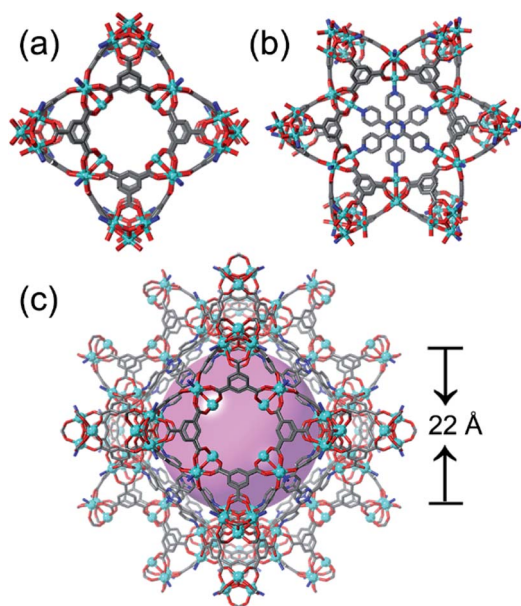

Fig. 2 The ball-and-stick representation of the square (a) and hexagonal (b) windows and a mesoporous cage (c) in the ST-**sod**-MOF structure. Hydrogen atoms and coordinated water molecules have been omitted for clarity; atom color scheme is as follows: metal = turquoise, C = gray, O = red, and N = blue. The light pink ball represents the largest sphere that can fit inside the cage with consideration for the van der Waals radii of the nearest atoms.

connected network with the point symbol $(4^3)_6(4^6 \cdot 6^{15} \cdot 8^7)_3(6^3)_2$ (Fig. S4†). However, this initial simplification cannot clearly explain the entire structure of ST-**sod**-Co. Alternatively, we could ignore the pair of staggered tpt ligands and consider the four

cobalt trimers connected *via* four btc ligands as the crux for ST formation, which was subsequently linked to the other STs in a corner-sharing fashion; as a result, the topology of the **sod** zeolitic network could be represented as $(4^2 \cdot 6^4)$ (Fig. 1d and S5†). To the best of our knowledge, this is the first example of a **sod** zeolitic network using corner-sharing, metal trimer-based supertetrahedra.[39,40]

For a better understanding of the role of tpt ligand on the assembly, a series of prototypical zeolitic ST-**sod**-MOFs were prepared. Like MIL-100 materials, the metal trimers are interconnected by the tricarboxylate linkers located in the faces to form ST, that extend into a three-dimensional zeolitic **mtn** topology with pentagonal and hexagonal pore windows. We also tried best to utilize such only ST vertices to obtain **sod** type MOFs with all open windows but without success. The reactions were carried out using the same protocol but without the use of tpt ligand; the self-assembly of single inorganic salt CoSO$_4$·7H$_2$O or Ni(NO$_3$)$_2$·6H$_2$O and btc ligand led to the formation of unknown crystalline phases (Fig. S10†); while using mixed inorganic salts CoCl$_2$·6H$_2$O and Cp$_2$TiCl$_2$ with btc ligand produced a previously reported porous Co-BTC framework without Ti^{4+} cations (Fig. S11†).[41] These experiments suggest that there appears to be a dominant structure-determining driving force of a pair of staggered tpt ligands acting as the window-space-directed agent leading to the formation of zeolitic mesoporous ST-**sod**-MOFs.

Thermogravimetric analysis revealed that ST-**sod**-Co, ST-**sod**-Ni, and ST-**sod**-Co/Ti were thermally stable up to 320, 350, and 380 °C in N$_2$ stream, respectively (Fig. S15†). Furthermore, *in situ* variable-temperature PXRD patterns of ST-**sod**-Ni and ST-**sod**-Co/Ti under air confirmed the maintenance of their

framework integrity up to 300 and 320 °C, respectively (Fig. S12†). The higher thermal stability of ST-**sod**-Co/Ti was probably due to the presence of stronger Ti(IV)–O coordination bonds. The phase purities of the ST-**sod**-MOFs were confirmed *via* PXRD (Fig. S13†), which was also employed to assess the chemical stability of samples treated in water, hydrochloric acid solution (pH = 2), and sodium hydroxide solution (pH = 12) at 25 and 100 °C for 24 h. Notably, the PXRD patterns of ST-**sod**-Co/Ti remained intact after various treatments and were in good agreement with the calculated patterns obtained from single crystal data, indicating the retention of crystallinity and structural integrity of ST-**sod**-Co/Ti (Fig. 3a and b). In addition, the stability of ST-**sod**-Co/Ti was also confirmed by N_2 adsorption measurements. The adsorption capacities after water treatment under different conditions showed negligible changes as compared to the pristine sample (Fig. 3c). These results suggested that the Ti^{4+}/Co^{2+} cooperative crystallization strategy increased the resistance of the framework against hydrolysis. Similar features have also been reported in heterometallic crystalline porous materials.[19,20,35]

The porosity of the ST-**sod**-MOFs was assessed by performing N_2 sorption measurements at 77 K (Fig. 3d). Both the adsorption and desorption curves of all samples exhibited a reversible Type-I adsorption behavior with a stepwise N_2 adsorption isotherm, which is indicative of a mesoporous cage in the framework.[42] The saturated uptake values of 376, 400, and 457 cm^3 g^{-1} were obtained for ST-**sod**-Co, ST-**sod**-Ni, and ST-**sod**-Co/Ti, respectively, with corresponding BET surface areas of 1767, 1783, and 2362 m^2 g^{-1}, respectively (Fig. S16–S18†). In particular, the BET surface area of ST-**sod**-Co/Ti was superior to those

of other **sod**-type MOFs such as ZIF-8,[25,26] IFMC-1,[43] TTF-4,[44] CPM-8S,[45] and M-BTT (M = Mn, Fe, Co, Cu, Cd; BTT = 1,3,5-benzenetristetrazolate);[46] the value is also slightly larger than those of well-known ST-based porous materials such as MIL-143,[23] CAU-42,[24] PCN-777,[47] MOF-808,[48] MOF-818,[49] and sph-MOF-4.[50] The pore volumes of ST-**sod**-Co, ST-**sod**-Ni, and T-**sod**-Co/Ti were as 0.62, 0.62, and 0.71 cm^3 g^{-1}, respectively, which were in good agreement with the corresponding theoretical values of 0.65, 0.73, and 0.65 cm^3 g^{-1}, respectively, calculated using the PLATON program. Furthermore, the pore size distributions of the ST-**sod**-MOFs were calculated using the Horvath–Kawazoe (H–K) model assuming the sphere pore geometry, whose result indicates two types of pores with diameters of approximately 5.0 and 22.0 Å (Fig. 3d). These calculated values were in agreement with the effective cavity diameters of the small tetrahedral cage and the large truncated octahedral cage, respectively, as observed in the crystal structure *via* SCXRD.

The permanent porosity and distinctive cage structure of the three isostructural MOFs in this study encouraged us to examine their selective gas adsorption performance toward acetylene (C_2H_2), ethane (C_2H_6), ethylene (C_2H_4), carbon dioxide (CO_2), and methane (CH_4). First, single-component adsorption isotherms of the five gases were obtained at 273 and 298 K, where the adsorption capacities of all three isostructural MOFs followed the trend of $C_2H_2 > C_2H_6 > C_2H_4 \approx CO_2 \gg CH_4$ under the same conditions (Fig. S19–S21†).

Considering that the removal of CO_2 impurities to obtain high-purity C_2H_2 is highly desirable in industrial applications, the process of C_2H_2/CO_2 separation is an important albeit difficult industrial separation process because of the
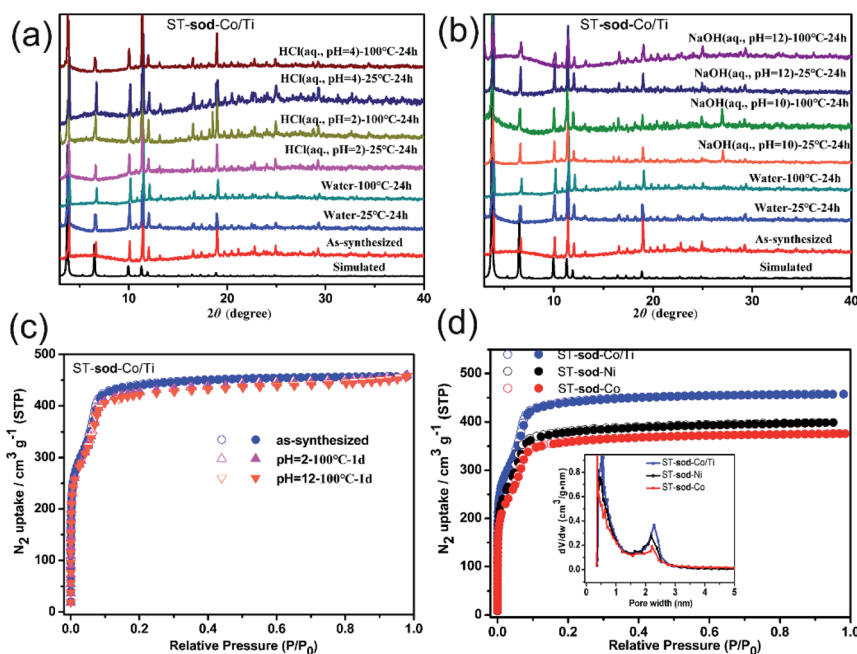

Fig. 3 (a and b) PXRD patterns for ST-**sod**-MOFs after being exposed to aqueous, acidic, and basic conditions at 25 and 100 °C for 24 h. (c) Comparison of the N_2 adsorption isotherms at 77 K of the as-synthesized ST-**sod**-MOFs and after water treatment under pH 2 and 12 at 100 °C for 24 h. (d) N_2 adsorption isotherm at 77 K for adsorption (solid circles), desorption (hollow circles), and the corresponding pore size distributions (inset) of ST-**sod**-MOFs featuring metallic trimers comprising Co (red), Ni (black), and Co/Ti (blue).

similarities in molecular size and physicochemical characteristics of C_2H_2 and CO_2.[51] Fig. 4 shows the results of separation using ST-**sod**-Co/Ti, which was chosen from the three MOF types examined because it exhibited the highest BET surface area and thermal/chemical stability. The adsorption capacity values of ST-**sod**-Co/Ti for C_2H_2 and CO_2 at 1.0 bar and 273 K were 105 and 72 cm^3 g^{-1}, respectively; at 298 K and 1.0 bar, these values were 57 and 40 cm^3 g^{-1}, respectively (Fig. 4a). The resulting C_2H_2/CO_2 uptake ratio of 1.42 for ST-**sod**-Co/Ti at 298 K and 1.0 bar was comparable to the results obtained for UTSA-74a (1.52)[52] and higher than those of benchmark MOFs such as TIFSIX-2-Cu-i (0.95),[53] SIFSIX-3-Ni (1.2),[54] and KMOF-1-Ni (1.19)[55] under the same conditions. The adsorption selectivity of ST-**sod**-Co/Ti for equimolar binary C_2H_2/CO_2 gas mixtures was evaluated using the ideal adsorbed solution theory based on a single-site Langmuir–Freundlich simulation on the pure-component isotherms of C_2H_2 and CO_2 at 273 and 298 K (Fig. 4b). The adsorption selectivity value of ST-**sod**-Co/Ti at 298 K was 2.66 at 0.01 bar, which decreased with increasing pressure to 1.65 at 1.0 bar. We noted that the C_2H_2/CO_2 selectivity value of 1.65 for ST-**sod**-Co/Ti at 298 K and 1.0 bar was lower than those of prototypic MOFs such as FJU-90 (4.3),[34] TIFSIX-2-Cu-i (6.5),[53] and UTSA-74a (9.0),[52] but was comparable to that of Zn-MOF-74 (2.0)[52] under similar conditions. The adsorption isotherms of C_2H_2 and CO_2 at 273 and 298 K were fitted using the virial equation (Fig. S22–S27†), and the isosteric heat (Q_{st}) was calculated using the Clausius–Clapeyron equation. The zero-coverage Q_{st} value of C_2H_2 for ST-**sod**-Co/Ti was calculated to be 42.4 kJ mol^{-1}, which was much larger than that for CO_2 of

33.6 kJ mol^{-1} (Fig. S28†). This discrepancy between the Q_{st} values may be attributed to the synergistic effects exerted by the ultramicroporous apertures, the open metal sites, and the uncoordinated triazine N-atoms lined on the pores surfaces. Notably, the zero-coverage Q_{st} value for C_2H_2 in ST-**sod**-Co/Ti (42.4 kJ mol^{-1}) was at the higher end of the scale for MOF-based solid adsorbents (>40 kJ mol^{-1})[55] and was much higher than those observed for ST-**sod**-Ni (25.2 kJ mol^{-1}) and ST-**sod**-Co (29.1 kJ mol^{-1}) as well as the values associated with many other benchmark MOFs, including UTSA-74a (32 kJ mol^{-1}),[52] JCM-1 (36.9 kJ mol^{-1}),[56] and DICRO-4-Ni-i (37.7 kJ mol^{-1}),[57] albeit significant lower than an acetylene nanotrap Cu-ATC (79.1 kJ mol^{-1}) reported very recently.[58] However, the Q_{st} value for CO_2 in ST-**sod**-Co/Ti (33.6 kJ mol^{-1}) was similar to that observed for ST-**sod**-Ni (31.1 kJ mol^{-1}), ST-**sod**-Co (32.1 kJ mol^{-1}), JCM-1 (33.4 kJ mol^{-1}),[56] and DICRO-4-Ni-i (33.9 kJ mol^{-1}).[57] These results showed that there were more extensive interactions with C_2H_2 than CO_2, thereby rendering the potential application of ST-**sod**-Co/Ti for C_2H_2/CO_2 separation.

The C_2H_2/CO_2 separation capability of ST-**sod**-Co/Ti in practical applications was investigated *via* mixed-gas breakthrough experiments conducted at 298 K. In these breakthrough experiments, a mixed gas of C_2H_2/CO_2 (50 : 50, v/v) at a total flow of 1 mL min^{-1} was injected into a column packed with activated ST-**sod**-Co/Ti. The resulting breakthrough curve indicated that the CO_2 gas was the first eluted through the packed column after about 36.6 min g^{-1}, whereas the C_2H_2 gas was not detected until 42.5 min g^{-1} (Fig. 4c). This result
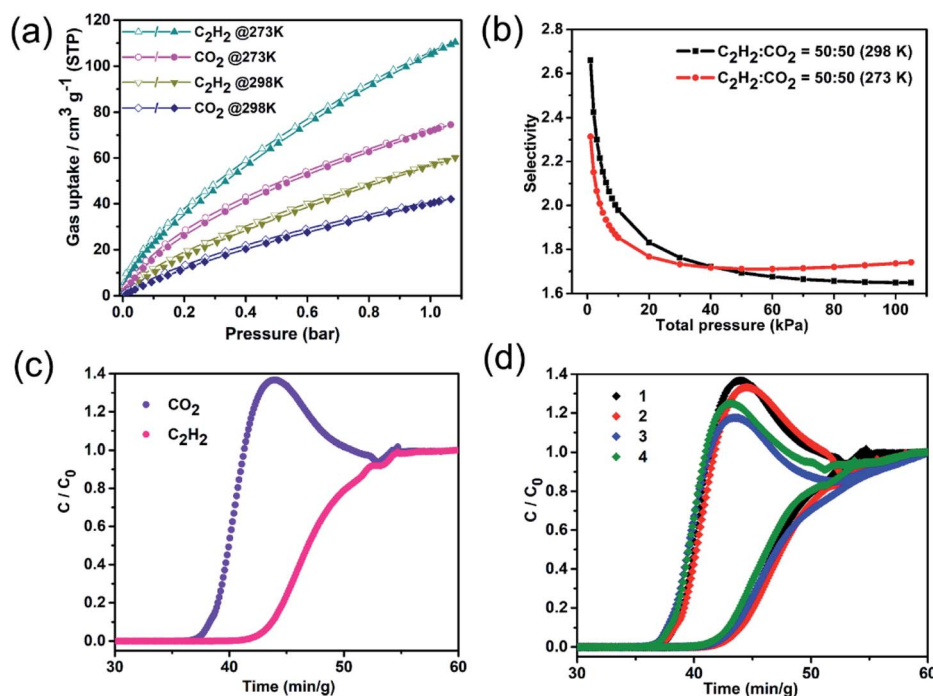

Fig. 4 (a) Single-component gas adsorption isotherms for C_2H_2 and CO_2 of ST-**sod**-Co/Ti measured at 273 K and 298 K. (b) IAST calculations of C_2H_2/CO_2 adsorption selectivity for ST-**sod**-Co/Ti at 273 K and 298 K. (c) Experimental column breakthrough curves of ST-**sod**-Co/Ti for an equimolar C_2H_2/CO_2 mixture at 298 K and 1.0 bar. (d) The cycling test of an equimolar C_2H_2/CO_2 mixture at 298 K and 1.0 bar.

demonstrated that activated ST-**sod**-Co/Ti could effectively capture C_2H_2 from an equimolar C_2H_2/CO_2 mixture *via* a packed column. Furthermore, the stability and recyclability of activated ST-**sod**-Co/Ti were examined using recycling breakthrough experiments. As shown in Fig. 4d, the activated ST-**sod**-Co/Ti was reusable for four cycles with no loss in its adsorption capacity, indicating that the MOF exhibited good regenerability for C_2H_2/CO_2 separation. Thus, ST-**sod**-Co/Ti holds some promise for the challenging application of C_2H_2/CO_2 separation.

Conclusions

In conclusion, we present a novel window-space-directed assembly strategy for the synthesis of zeolitic mesoporous MOFs with ultramicroporous apertures based on super-tetrahedral building units. Three isostructural ST-based ST-**sod**-MOFs, namely, ST-**sod**-Co, ST-**sod**-Ni, and ST-**sod**-Co/Ti, with homo- or heterometallic trimers were fabricated and characterized *via* SCXRD. Notably, the ST-**sod**-MOFs possessed a **sod** topology whose STs served as nodes. In these ST-**sod**-MOFs, the large β-cavity mesoporous pores (~22 Å diameter) were accessible *via* six square windows with ultramicroporous apertures (~5.6 Å diameter), whereas their eight hexagonal windows were closed by the paired tpt ligands acting as window-space-directed agents. Remarkably, ST-**sod**-Co/Ti exhibited good thermal stability, high acid/base-proof stability, and the ability to effectively separate C_2H_2/CO_2 mixtures. Like other heterometallic MOFs with variable metal trimers, this ST-**sod**-MOFs platform also exhibited enhanced chemical and functional complexity by tuning the metal cations. Thus, our study provides an effective and innovative strategy for building ST-based zeolitic mesoporous MOFs with ultramicroporous apertures and paves the way for the future design and synthesis of functional, highly connected materials for various applications.

Author contributions

L. Z., C. L., and S. M conceived the research. H. Y. synthesized samples. L. Z., F. L., J. Y., N. H., Q. W., and J. S., performed the syntheses and structural characterizations of MOFs. W. C., W. W., X. W., W. Y. and D. Y. performed the gas sorption and breakthrough experiments. Y. L. performed the SEM characterizations. L. Z. A. N., A. M. A. and S. M. wrote the manuscript. All authors contributed to the discussion.

Conflicts of interest

There are no conflicts to declare.

Acknowledgements

References

1 H. C. Zhou and S. Kitagawa, *Chem. Soc. Rev.*, 2014, **43**, 5415–5418.

2 X. Zhao, Y. Wang, D. S. Li, X. Bu and P. Feng, *Adv. Mater.*, 2018, **30**, 1705189.

3 R.-B. Lin, S. Xiang, W. Zhou and B. Chen, *Chem*, 2020, **6**, 337–363.

4 J. Liu, L. Chen, H. Cui, J. Zhang, L. Zhang and C. Y. Su, *Chem. Soc. Rev.*, 2014, **43**, 6011–6061.

5 Z. Niu, W. D. C. Bhagya Gunatilleke, Q. Sun, P. C. Lan, J. Perman, J.-G. Ma, Y. Cheng, B. Aguila and S. Ma, *Chem*, 2018, **4**, 2587–2599.

6 Y. Chen, V. Lykourinou, C. Vetromile, T. Hoang, L. J. Ming, R. W. Larsen and S. Ma, *J. Am. Chem. Soc.*, 2012, **134**, 13188–13191.

7 X. Lian, Y. P. Chen, T. F. Liu and H. C. Zhou, *Chem. Sci.*, 2016, **7**, 6969–6973.

8 M. Li, D. Li, M. O'Keeffe and O. M. Yaghi, *Chem. Rev.*, 2014, **114**, 1343–1370.

9 Y. Wang, L. Feng, W. Fan, K. Y. Wang, X. Wang, X. Wang, K. Zhang, X. Zhang, F. Dai, D. Sun and H. C. Zhou, *J. Am. Chem. Soc.*, 2019, **141**, 6967–6975.

10 X. J. Kong, T. He, Y. Z. Zhang, X. Q. Wu, S. N. Wang, M. M. Xu, G. R. Si and J. R. Li, *Chem. Sci.*, 2019, **10**, 3949–3955.

11 H. Jiang, J. Jia, A. Shkurenko, Z. Chen, K. Adil, Y. Belmabkhout, L. J. Weselinski, A. H. Assen, D.-X. Xue, M. O'Keeffe and M. Eddaoudi, *J. Am. Chem. Soc.*, 2018, **140**, 8858–8867.

12 B. Ortin-Rubio, H. Ghasempour, V. Guillerm, A. Morsali, J. Juanhuix, I. Imaz and D. Maspoch, *J. Am. Chem. Soc.*, 2020, **142**, 9135–9140.

13 J. J. T. Perry, J. A. Perman and M. J. Zaworotko, *Chem. Soc. Rev.*, 2009, **38**, 1400–1417.

14 V. Guillerm, D. Kim, J. F. Eubank, R. Luebke, X. Liu, K. Adil, M. S. Lah and M. Eddaoudi, *Chem. Soc. Rev.*, 2014, **43**, 6141–6172.

15 G. Férey, C. Serre, C. Mellot-Draznieks, F. Millange, S. Surblé, J. Dutour and I. Margiolaki, *Angew. Chem., Int. Ed.*, 2004, **116**, 6456–6461.

16 G. Ferey, C. Mellot-Draznieks, C. Serre, F. Millange, J. Dutour, S. Surble and I. Margiolaki, *Science*, 2005, **309**, 2040–2042.

17 A. C. Sudik, A. P. Côté, A. G. Wong-Foy, M. O'Keeffe and O. M. Yaghi, *Angew. Chem., Int. Ed.*, 2006, **45**, 2528–2533.

18 A. Schoedel and M. J. Zaworotko, *Chem. Sci.*, 2014, **5**, 1269–1282.

19 Q. G. Zhai, X. Bu, C. Mao, X. Zhao, L. Daemen, Y. Cheng, A. J. Ramirez-Cuesta and P. Feng, *Nat. Commun.*, 2016, **7**, 13645.

20 Q. G. Zhai, X. Bu, C. Mao, X. Zhao and P. Feng, *J. Am. Chem. Soc.*, 2016, **138**, 2524–2527.

21 S. Abednatanzi, P. Gohari Derakhshandeh, H. Depauw, F. X. Coudert, H. Vrielinck, P. Van Der Voort and K. Leus, *Chem. Soc. Rev.*, 2019, **48**, 2535–2565.

22 D. Feng, T. F. Liu, J. Su, M. Bosch, Z. Wei, W. Wan, D. Yuan, Y. P. Chen, X. Wang, K. Wang, X. Lian, Z. Y. Gu, J. Park, X. Zou and H. C. Zhou, *Nat. Commun.*, 2015, **6**, 5979.

23 H. Chevreau, T. Devic, F. Salles, G. Maurin, N. Stock and C. Serre, *Angew. Chem., Int. Ed.*, 2013, **52**, 5056–5060.

24 S. Leubner, V. E. G. Bengtsson, A. K. Inge, M. Wahiduzzaman, F. Steinke, A. Jaworski, H. Xu, S. Halis, P. Ronfeldt, H. Reinsch, G. Maurin, X. Zou and N. Stock, *Dalton Trans.*, 2020, **49**, 3088–3092.

25 X.-C. Huang, Y.-Y. Lin, J.-P. Zhang and X.-M. Chen, *Angew. Chem., Int. Ed.*, 2006, **45**, 1557–1559.

26 K. S. Park, Z. Ni, A. P. Côté, J. Y. Choi, R. Huang, F. J. Uribe-Romo, H. K. Chae, M. O'Keeffe and O. M. Yaghi, *Proc. Natl. Acad. Sci. U. S. A.*, 2006, **103**, 10186–10191.

27 C. Zhang, R. P. Lively, K. Zhang, J. R. Johnson, O. Karvan and W. J. Koros, *J. Phys. Chem. Lett.*, 2012, **3**, 2130–2134.

28 D. J. Babu, G. He, J. Hao, M. T. Vahdat, P. A. Schouwink, M. Mensi and K. V. Agrawal, *Adv. Mater.*, 2019, **31**, e1900855.

29 K. Adil, Y. Belmabkhout, R. S. Pillai, A. Cadiau, P. M. Bhatt, A. H. Assen, G. Maurin and M. Eddaoudi, *Chem. Soc. Rev.*, 2017, **46**, 3402–3430.

30 S. Shalini, S. Nandi, A. Justin, R. Maity and R. Vaidhyanathan, *Chem. Commun.*, 2018, **54**, 13472–13490.

31 S. T. Zheng, J. T. Bu, Y. Li, T. Wu, F. Zuo, P. Feng and X. Bu, *J. Am. Chem. Soc.*, 2010, **132**, 17062–17064.

32 Q. G. Zhai, X. Bu, X. Zhao, D. S. Li and P. Feng, *Acc. Chem. Res.*, 2017, **50**, 407–417.

33 X. Zhao, X. Bu, Q. G. Zhai, H. Tran and P. Feng, *J. Am. Chem. Soc.*, 2015, **137**, 1396–1399.

34 Y. Ye, Z. Ma, R. B. Lin, R. Krishna, W. Zhou, Q. Lin, Z. Zhang, S. Xiang and B. Chen, *J. Am. Chem. Soc.*, 2019, **141**, 4130–4136.

35 H. Yang, Y. Wang, R. Krishna, X. Jia, Y. Wang, A. N. Hong, C. Dang, H. E. Castillo, X. Bu and P. Feng, *J. Am. Chem. Soc.*, 2020, **142**, 2222–2227.

36 M. Fujita, D. Oguro, M. Miyazawa, H. Oka, K. Yamaguchi and K. Ogura, *Nature*, 1995, **378**, 469–471.

37 L. Zhang, J. Qian, W. Yang, X. Kuang, J. Zhang, Y. Cui, W. Wu, X.-Y. Wu, C.-Z. Lu and W.-Z. Chen, *J. Mater. Chem. A*, 2015, **3**, 15399–15402.

38 X. T. Liu, K. Wang, Z. Chang, Y. H. Zhang, J. Xu, Y. S. Zhao and X. H. Bu, *Angew. Chem., Int. Ed.*, 2019, **58**, 13890–13896.

39 M. Eddaoudi, D. F. Sava, J. F. Eubank, K. Adil and V. Guillerm, *Chem. Soc. Rev.*, 2015, **44**, 228–249.

40 Y. X. Tan, F. Wang and J. Zhang, *Chem. Soc. Rev.*, 2018, **47**, 2130–2144.

41 C. N. Dzesse T, E. N. Nfor and S. A. Bourne, *Polyhedron*, 2020, **189**, 114724.

42 N. Klein, I. Senkovska, K. Gedrich, U. Stoeck, A. Henschel, U. Mueller and S. Kaskel, *Angew. Chem., Int. Ed.*, 2009, **48**, 9954–9957.

43 J. S. Qin, J. C. Zhang, M. Zhang, D. Y. Du, J. Li, Z. M. Su, Y. Y. Wang, S. P. Pang, S. H. Li and Y. Q. Lan, *Adv. Sci.*, 2015, **2**, 1500150.

44 Y. H. Tang, F. Wang, J. X. Liu and J. Zhang, *Chem. Commun.*, 2016, **52**, 5625–5628.

45 Y. Gai, X. Chen, H. Yang, Y. Wang, X. Bu and P. Feng, *Chem. Commun.*, 2018, **54**, 12109–12112.

46 E. D. Bloch, W. L. Queen, M. R. Hudson, J. A. Mason, D. J. Xiao, L. J. Murray, R. Flacau, C. M. Brown and J. R. Long, *Angew. Chem., Int. Ed.*, 2016, **55**, 8605–8609.

47 D. Feng, K. Wang, J. Su, T. F. Liu, J. Park, Z. Wei, M. Bosch, A. Yakovenko, X. Zou and H. C. Zhou, *Angew. Chem., Int. Ed.*, 2015, **54**, 149–154.

48 H. Furukawa, F. Gandara, Y. B. Zhang, J. Jiang, W. L. Queen, M. R. Hudson and O. M. Yaghi, *J. Am. Chem. Soc.*, 2014, **136**, 4369–4381.

49 Q. Liu, Y. Song, Y. Ma, Y. Zhou, H. Cong, C. Wang, J. Wu, G. Hu, M. O'Keeffe and H. Deng, *J. Am. Chem. Soc.*, 2019, **141**, 488–496.

50 H. Jiang, J. Jia, A. Shkurenko, Z. Chen, K. Adil, Y. Belmabkhout, L. J. Weselinski, A. H. Assen, D. X. Xue, M. O'Keeffe and M. Eddaoudi, *J. Am. Chem. Soc.*, 2018, **140**, 8858–8867.

51 C. R. Reid and K. M. Thomas, *J. Phys. Chem. B*, 2001, **105**, 10619–10629.

52 F. Luo, C. Yan, L. Dang, R. Krishna, W. Zhou, H. Wu, X. Dong, Y. Han, T. L. Hu, M. O'Keeffe, L. Wang, M. Luo, R. B. Lin and B. Chen, *J. Am. Chem. Soc.*, 2016, **138**, 5678–5684.

53 K.-J. Chen, H. S. Scott, D. G. Madden, T. Pham, A. Kumar, A. Bajpai, M. Lusi, K. A. Forrest, B. Space, J. J. Perry and M. J. Zaworotko, *Chem*, 2016, **1**, 753–765.

54 Y. L. Peng, T. Pham, P. Li, T. Wang, Y. Chen, K. J. Chen, K. A. Forrest, B. Space, P. Cheng, M. J. Zaworotko and Z. Zhang, *Angew. Chem., Int. Ed.*, 2018, **57**, 10971–10975.

55 S. Mukherjee, Y. He, D. Franz, S. Q. Wang, W. R. Xian, A. A. Bezrukov, B. Space, Z. Xu, J. He and M. J. Zaworotko, *Chem.–Eur. J.*, 2020, **26**, 4923–4929.

56 J. Lee, C. Y. Chuah, J. Kim, Y. Kim, N. Ko, Y. Seo, K. Kim, T. H. Bae and E. Lee, *Angew. Chem., Int. Ed.*, 2018, **57**, 7869–7873.

57 H. S. Scott, M. Shivanna, A. Bajpai, D. G. Madden, K. J. Chen, T. Pham, K. A. Forrest, A. Hogan, B. Space, J. J. Perry Iv and M. J. Zaworotko, *ACS Appl. Mater. Interfaces*, 2017, **9**, 33395–33400.

58 Z. Niu, X. Cui, T. Pham, G. Verma, P. C. Lan, C. Shan, X. Xing, K. A. Forrest, S. Suepaul, B. Space, A. M. Al-Enizi, A. Nafady and S. Ma, *Angew. Chem., Int. Ed.*, 2021, **60**, 5283–5288.